Electronic Structure and Field Emission Properties of Double-Walled Carbon Nanotubes Synthesized by Hydrogen Arc Discharge

ARTICLE *in* THE JOURNAL OF PHYSICAL CHEMISTRY C · DECEMBER 2007

Impact Factor: 4.77 · DOI: 10.1021/jp0768468

4 AUTHORS, INCLUDING:

Byeongchul Ha
Incheon National University
17 PUBLICATIONS **227** CITATIONS

Electronic Structure and Field Emission Properties of Double-Walled Carbon Nanotubes Synthesized by Hydrogen Arc Discharge

Byeongchul Ha,[†] Dong Hoon Shin,[‡] Jeunghee Park,[§] and Cheol Jin Lee*[,‡]

Department of Nano Science, Cheongju University, Cheongju, 360-764, Korea, School of Electrical Engineering, Korea University, Seoul 136-713, Korea, and Department of Chemistry, Korea University, Jochiwon 339-700, Korea

Received: August 27, 2007; In Final Form: October 11, 2007

We have synthesized high-purity double-walled carbon nanotubes (DWCNTs) by an arc-discharge method in hydrogen ambient. The DWCNTs were synthesized using a mixture of Fe catalyst and FeS promoter. Without FeS promoter, we only obtained single-walled carbon nanotubes (SWCNTs). The synthesized DWCNTs had outer diameters in the range of 3.0−3.4 nm and an average interlayer distance of 0.38 nm between graphene layers. The FeS promoter played a key role for the DWCNT growth. The DWCNTs indicated high electronic density of states in the binding energy region between 3.88 and 13.23 eV below Fermi energy, indicating that the DWCNTs had alot of delocalized graphite σ and σ/π electrons. For field emission properties, the typical turn-on field of DWCNTs was about 3.0 V/μm at the emission current density of 0.1 μA/cm^2, and the emission current density of DWCNTs was about 10 mA/cm^2 at the applied field of 6.5 V/μm. It is considered that the higher current densities of DWCNTs were mainly attributed to the emitted delocalized graphite σ and σ/π state electrons of DWCNTs. Moreover, DWCNTs have higher emission stability than SWCNTs due to two neighboring graphene layers.

1. Introduction

Since first discovery of carbon nanotubes (CNTs), there have been many reports on the synthesis and characterization of various CNTs, such as single-walled carbon nanotubes (SWCNTs), double-walled carbon nanotubes (DWCNTs), and multiwalled carbon nanotubes (MWCNTs). Recently, much attention has been focused on DWCNTs because they are composed of two concentric cylindrical graphene layers, showing interesting geometries for electrical and mechanical properties.[1−5] More recently, several groups have reported the synthesis of DWCNTs using catalytic chemical vapor deposition (CCVD)[6−8] or arc-discharge methods.[9−12]

Compared with SWCNTs, DWCNTs can provide advanced electrical and mechanical properties, structural stability, and thermal conductivity due to their coaxial structure.[13] Thus, the DWCNTs can offer numerous applications because they have outstanding field-emission properties, high chemical inertness, thermal conductivity, and high mechanical stiffness.[13−19] Among the various applications, the field emission application is interesting because DWCNTs can possess excellent field-emission properties, indicating merits of both SWCNTs and MWCNTs. The DWCNTs may show low threshold voltage for electron emission as for SWCNTs, and good lifetime-emission stability as for MWCNTs.[20] Furthermore, some research groups reported that the electronic structure of CNTs has an effect on the electron field emission and the electronic transport properties of CNTs.[21−23] There have been several reports on the electronic structure of SWCNTs.[23,24] We also investigated a relationship between the field emission properties and the electronic structure of SWCNTs.[23] However, there has been no report on the electronic structures of DWCNTs yet. Photoemission spectroscopy can present the information about electronic structure over a wide energy range including core levels. In this work, we evaluated the field emission properties and investigated the electronic structures of DWCNTs produced by a hydrogen arc-discharge method. Furthermore, we studied the field emission properties dependent on the electronic structure of DWCNTs.

2. Experimental Section

High-purity DWCNTs or SWCNTs were synthesized by a conventional dc arc-discharge method in a stainless steel chamber. The anode was a graphite rod (6 mm in diameter) with a drilled hole (3 mm in diameter and 300 mm in length) filled with the mixture of iron metal catalyst, graphite powder, and FeS as promoter. The amount of Fe catalyst with respect to graphite powder was fixed. The amount of FeS promoter with respect to Fe catalyst was varied to 100, 50, 20, 10 (wt%) as shown in Table 1. The fixed cathode was a pure graphite rod. A vacuum chamber was always cooled by circulated water. In order to generate arc plasma, a gap between two electrodes was maintained with a constant distance of 1 mm. Hydrogen was used as a buffer gas. Pressure was kept at various ranges from 250 to 450 Torr. The discharge current was also used at various ranges from 30 to 70 A. The duration of arc-discharge process was 20 min. Web-like carbon materials were obtained around the cathode after evaporation.

The as-synthesized DWCNTs were purified using a thermal oxidation at 450 °C for 1 h inside a furnace system in an air atmosphere in order to remove amorphous carbon materials and catalyst particles on the surface of CNTs. After oxidation, we carried out homogenization (homogenizer, IKA, DI-25 basic yellow line) operated at 8500 rpm for 10 min in 7% HCl solution to remove metallic-catalyst particles. Finally, the purified

* Corresponding author. E-mail: cjlee@korea.ac.kr. Tel: +82-2-3290-3216. Fax: +82-2-921-4722.
[†] Cheongju University.
[‡] School of Electrical Engineering, Korea University.
[§] Department of Chemistry, Korea University.

10.1021/jp0768468 CCC: $40.75
Published on Web 12/22/2007

TABLE 1: Selectivity, Yield, and Purity of DWCNTs Dependent on Process Conditions

no.	FeS/Fe (ratio)	pressure of buffer gas H_2 (Torr)	current (A)	product (CNT)	yield (mg)	purity
1	1	250	60	DWCNT	300	very low
2	0.5	250	60	DWCNT	200	low
3	0.2	250	60	DWCNT	350	middle
4	0.2	350	60	DWCNT	250	high
5	0.2	450	50	DWCNT	250	middle
6	0.2	450	70	DWCNT	300	middle
7	0.2	450	60	DWCNT	400	very high
8	0.1	450	60	SWCNT	250	very high
9	0	450	60	SWCNT	350	very high

DWCNTs were collected by membrane filtration (pore size: 0.2 μm) and washed with DI-water several times. We treated the produced SWCNTs using the same process as that used for the DWCNTs.

To measure field emission from the DWCNTs, the produced DWCNTs were purified using thermal oxidation and chemical treatment. The entangled DWCNTs were dispersed in ethanol solution using ultrasonication. Then, the suspension containing DWCNTs was sprayed on the Ti(300 nm)/Cr(300 nm)/n-Si substrate for 8 min using a spray gun. The substrate was dried in air, followed by baking at 400 °C for 20 min using a rapid thermal annealing to maintain a good ohmic contact between DWCNTs and substrates. We also prepared SWCNTs like DWCNTs to evaluate the field emission properties.[23] Field-electron-emission measurements were performed in a vacuum chamber at a pressure of less than 1×10^{-6} Torr. The cathode was a Ti/Cr film-deposited n-type silicon substrate and the anode was a copper plate. The gap between the cathode and the anode was about 300 μm, and the measured emission area was 7 mm^2. Emission current was monitored with a Keithley 6517A and recorded at intervals of 0.5 s.

As-synthesized and purified DWCNTs were characterized by scanning electron microscopy (SEM) (Hitachi, S-4700), transmission electron microscopy (TEM) (FEI Company, Tecnai F2O), and Raman spectroscopy (Bruker, RFS-100/S, Nd:YAG-laser excitation, laser-beam wavelength: 1064 nm).

The photoemission measurements were performed at the U7 beam line of the Pohang Light Source (PLS). The U7 beam line was designed to provide soft X-rays in the energy range of 50−1500 eV. The XPS data were collected using the photon energy of 1265 eV. The spectral-resolving power ($E/\Delta E$) of incident photons is 4000−5000 at all energy ranges. The background was subtracted by Shirley's method. The experiment was performed in an ultrahigh vacuum chamber with a base pressure of less than 5×10^{-10} Torr. The photoelectrons emitted from the surface of sample were analyzed with an energy analyzer (Physical Electronics: Model PHI 3057 with a 16-channel detector). The analyzer was located at 55° from the surface normal.

3. Results and Discussion

3.1. Synthesis and Characterization of DWCNTs. Figure 1a,b shows the low-magnification SEM images of as-synthesized carbon materials using arc discharge. A lot of paper-like carbon materials were produced at the reactor chamber as shown in Figure 1a. Figure 1c indicates the high-magnification SEM image of the as-synthesized carbon materials. The as-synthesized carbon materials show high-purity CNTs without amorphous carbon deposits or carbon flakes even though some catalyst metal particles (white spots) exist among the carbon products. Figure 1d shows the high-magnification SEM image of the CNTs after thermal oxidation and chemical acid treatment. The purified CNTs indicate clean and smooth morphology with a high density of bundles. In addition, the purified CNTs reveal increased bundle diameters of several tens of nanometers due to van der Waals force between the bundles during purification process.

Figure 2 shows the TEM images of the CNTs produced by the optimum condition of 20 wt% of FeS promoter with respect to Fe catalyst.

TEM shows that the as-synthesized carbon materials reveal DWCNTs with two graphite sheets as shown in Figure 2. The synthesized DWCNTs have outer diameters in the range of 3.0−3.4 nm and an average interlayer distance of 0.38 nm between graphene layers. The diameter of DWCNT bundles synthesized by arc discharge is larger than that of other group's DWCNTs synthesized by CCVD.[7] Most of the DWCNTs exist in a bundle shape as shown in Figure 2. However, we can sometimes see an isolated DWCNT with a diameter of 5.0 nm as shown in Figure 2c. In this work, from several TEM observations, we could find that the isolated DWCNTs generally have outer diameters that ranged from 4 to 6 nm and an interlayer spacing of about 0.4 nm. The outer diameter of DWCNTs is similar to the previous results, while interlayer spacing of DWCNTs is slightly larger than that of the other group's results.[25] The diameter of isolated DWCNTs is much larger than that of the individual DWCNT within bundles. The approximate proportion of DWCNTs was above 80% with respect to the total carbon materials (DWCNTs, SWCNTs).

We observe some catalyst nanoparticles and a few amorphous carbon materials on the surface of DWCNT bundles. In the TEM images (Figure 2a,c), catalyst particles are surrounded by the graphitic shell with one or several layers.

Figure 3 shows Raman spectra for the as-synthesized DWCNTs produced by the condition of 20 wt% FeS promoters. The Raman spectra of DWCNTs clearly indicate the main appearance of the D-band at 1271.2 cm^{-1} and the strong G-band at 1591.4 cm^{-1}. The G-band, the E_{2g} (stretching) mode of graphite, indicates an arrangement of the hexagonal lattice of graphite whereas the D-band indicates the level of disordered carbon. The small ratio of I(D)/I(G) reveals that the defect level in the atomic carbon structure is low, affording a high-quality DWCNT (where I is intensity). At low Raman shift frequencies, several peaks show radial breathing modes (RBM), resulting from different diameters of CNTs. The diameters of DWCNTs can be calculated by the expression $w = 6.5 + 223.75/d$.[4,26] According to the following correlation between frequency ω (cm^{-1}) and diameter d (nm), $d = 223.75/(\omega - 6.5)$ can be applicable to DWCNT bundles. Thus, the RBM peaks at 83.3, 102.6, 118, 147, 160.5, and 264.6 cm^{-1} of the DWCNT bundle correspond to the diameters of 2.913, 2.328, 2.006, 1.592, 1.452, and 0.886 nm, respectively. It is well-known that CNTs with a large diameter (>3 nm) exhibit a weak Raman cross-section so that we cannot detect the RBM frequencies of large diameters above 3 nm.[27] Therefore, it is very difficult to determine the real diameter of DWCNTs using a Raman analysis. However, we can estimate that the outer tube diameters of DWCNTs are in the range of 2.006−2.913 nm and the inner tube diameters are in the range of 0.866−1.592 nm even though DWCNTs with the same outer-tube diameter can have different inner-tube diameters because of the difference in chirality.[27] It is well-known that Raman analysis only gives us overall information of diameters of CNTs. According to HRTEM observation, our CNT samples indicated that the approximate proportion of

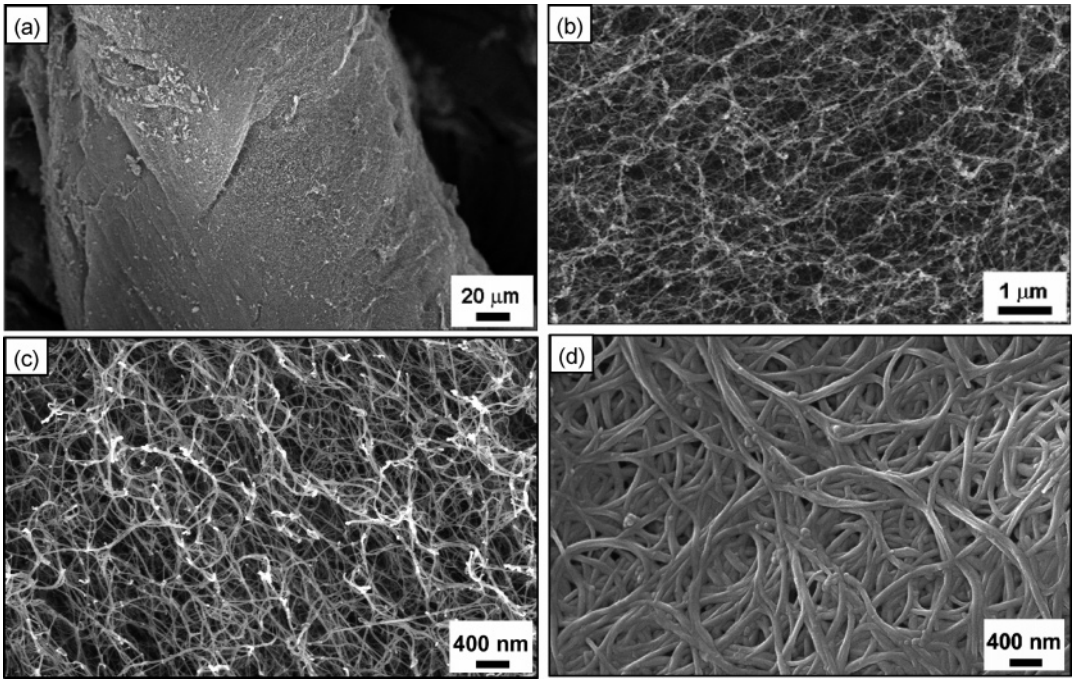

Figure 1. SEM micrographs of CNTs. (a−c) the as-synthesized CNTs. (d) the purified CNTs.

DWCNTs was above 80% with respect to the total carbon materials (DWCNTs, SWCNTs). Moreover, TEM observation showed that the synthesized DWCNTs have outer diameters in the range of 3.0−3.4 nm and an average interlayer distance of 0.38 nm between graphene layers. In this work, we only roughly calculated diameter of DWCNTs based on Raman peaks and the average interlayer distance of 0.38 nm. It is noteworthy that there clearly exist some SWCNTs with diameters of 0.866−1.592 nm.

Figure 4 shows a thermogravimetric analysis (TGA) of the DWCNTs after purification. As shown in Figure 4, TGA shows that the weight % of remaining carbon materials become 29.62 wt% at 858.8 °C, indicating the carbon yield about 70.38 wt%. The remaining materials mainly consist of Fe oxide materials and/or carbon balls introduced during the synthesis. It is still complicated to remove the Fe metal catalyst since the Fe metal catalyst is surrounded by several graphene layers in graphitic polyhedra. The derivative thermogravimetric (DTG) curve of TGA also shows that the produced carbon materials consist of a homogeneous carbon material and have a maximum oxidation temperature of 664.05 °C, affording highly crystalline DWCNTs.

We studied selectivity, yield, and purity of DWCNTs by adjusting process parameters and summarized the results in Table 1. As shown in Table 1, the highest yield and purity of DWCNTs were achieved under the condition of no. 7. When we increased the amount of FeS promoter more than 20 wt% with respect to Fe catalyst, the produced carbon materials mainly consisted of DWCNTs with a network morphology. On the other hand, when we decreased the amount of FeS promoter less than 20 wt% with respect to Fe catalysts, the produced carbon materials were not DWCNTs but SWCNTs.[23] In this case, we found that the produced carbon materials were composed of SWCNTs more than 90%.

There were some reports which indicated the synthesis of DWCNTs using sulfur promoter.[9,25,26,28−31] Hutchison et al. demonstrated that sulfur is not critical for the formation of DWCNTs but related to increasing the SWCNT yield.[9] On the other hand, some research groups announced that the sulfur additive has an effect to promote the formation of DWCNTs and also widen the diameter of SWCNTs.[25,28,29] In their results, there was no success in the synthesis of DWCNT without sulfur. It is still difficult to explain the exact role of the sulfur additive in the DWCNT synthesis. However, there are two kinds of understanding on the contribution of sulfur for the DWCNT growth. One is that the sulfur may increase the reactivity of the iron catalysts by forming Fe−S eutectic or by selectively poisoning the surface of the catalyst.[29] The other is that the formation of DWCNTs or increased diameter of SWCNTs from the action of the sulfur additive is mainly attributed to increased size of catalyst particles due to active agglomeration.[25,28] According to our experimental results, when the amount of FeS promoter was more than 20 wt% with respect to Fe catalyst, the carbon materials showed DWCNTs while SWCNTs were seen when the amount of FeS promoter was less than 20 wt% with respect to Fe catalyst. Thus, in this work, we consider that the main role of the sulfur additive is to encourage agglomeration of the Fe metal catalyst, resulting in the increased size of Fe catalyst particles. As a result, double carbon graphene layers appear on the Fe catalyst. Further study is necessary to understand the exact role of sulfur for the DWCNT growth. Here, we suggest that the addition of sulfur to the iron metal catalyst is essential for the DWCNT growth, and the type of CNTs, namely SWCNTs or DWCNTs, can be simply controlled by adjusting the concentration of FeS promoter with respect to Fe catalyst.

3.2. Photoemission Properties of DWCNTs. We investigated photoemission properties from the purified DWCNTs to understand the electronic structure of DWCNTs. As shown in the Figure 5a, the photoemission study reveals different characteristics between SWCNTs and DWCNTs in the C-1s core-level energy position and the full width at half-maximum (FWHM). The C-1s peaks of SWCNTs and DWCNTs are identified at the binding energy of 284.57 and 284.69 eV, respectively. The binding energy of DWCNTs is shifted to slightly higher energy by 0.12 eV compared with the SWCNTs. The DWCNTs also have a larger FWHM of 0.72 eV than that

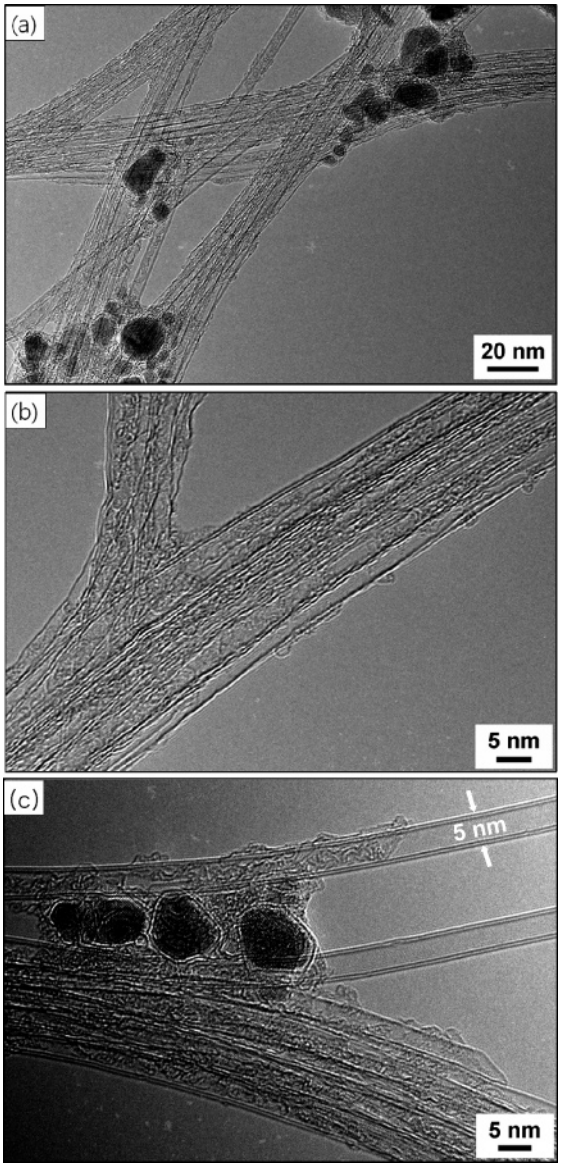

Figure 2. TEM micrographs of the as-synthesized DWCNTs. (a) TEM images of DWCNT bundles and isolated DWCNTs. (b, c) HRTEM image of isolated DWCNTs and DWCNT bundles.

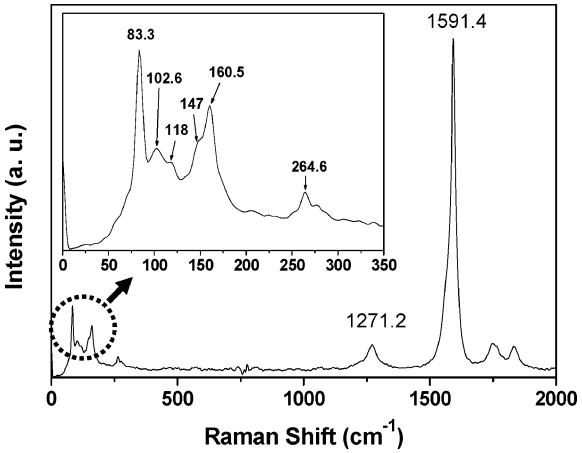

Figure 3. Raman spectra of the as-synthesized DWCNTs. The inset shows RBM modes.

of the SWCNTs of 0.67 eV. The positive 0.12 eV shift of the C-1s peak may be ascribed to the stronger carbon−carbon binding energy due to the interlayer of DWCNTs. The stronger

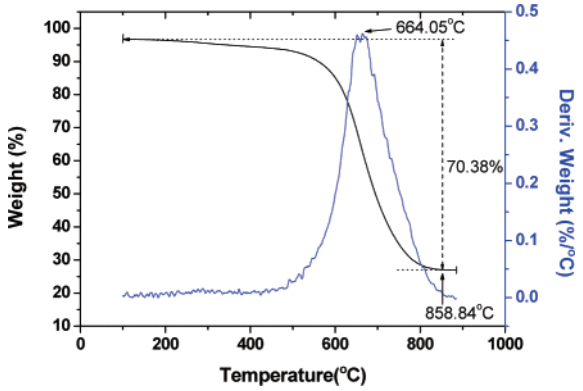

Figure 4. Thermogravimetric properties of the purified DWCNTs.

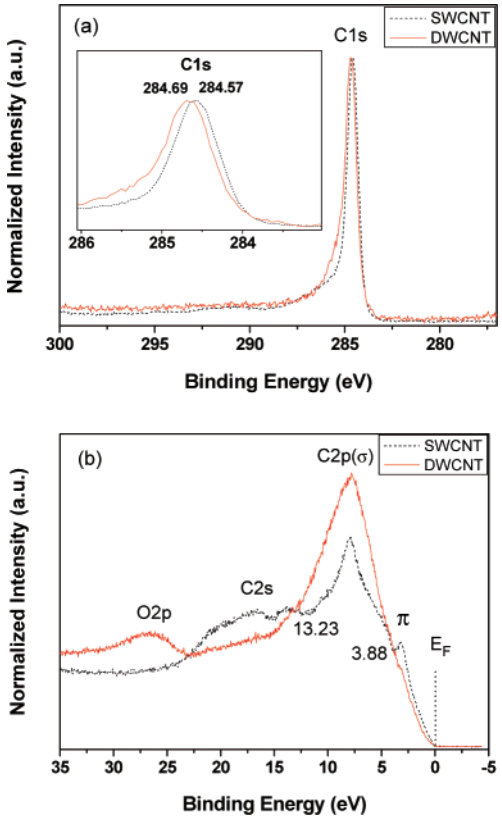

Figure 5. Photoemission from purified DWCNTs and SWCNTs,[23] respectively. (a) C-1s peak spectra of purified DWCNTs and SWCNTs. (b) The valence band of purified SWCNTs and DWCNTs. Fermi energy, E_F, is chosen at zero binding energy.

$c-c$ binding energy is probably attributed to the van der Waals interaction between two adjacent graphene layers.[15] The C-1s peaks at the binding energy of 284.57 and 284.69 eV indicate hybridized sp^2 carbons on the CNT walls, which are comparable to the C-1s binding energy of graphite. The tails near 286 eV of DWCNTs correspond to the C atoms at the defect sites.

As shown in Figure 5b, the 16.62 eV peak and the intense 7.89 eV peak of SWCNTs originate from the C-2s band and C-2p band, respectively. On the other hand, the peaks around 16.6 and 7.72 eV of DWCNTs originate from the C-2s band and C-2p band, respectively. In this work, the photoemission spectrum also shows an intense C-2p/C-2s feature at 13.68 eV in SWCNTs and a strong O-2s feature at ~26.1 eV in DWCNTs.

The valence-band spectrum of the DWCNTs is rather different from that of SWCNTs. The main difference in spectral features between the DWCNTs and SWCNTs appears in the energy region near Fermi level. The electronic density of states (DOS)

of DWCNTs in the binding energy region between 3.88 and 13.23 eV is clearly higher than that of SWCNTs, indicating that DWCNTs have more delocalized graphite σ and σ/π electrons than that of the SWCNTs. However, DWCNTs exhibit a slightly lower electronic DOS than SWCNTs in the binding energy region between 0 and 3.88 eV.

3.3. Field-Emission Properties of DWCNTs. Bonard et al.[18,32] examined the discrepancy of field emission properties of SWCNTs and MWCNTs due to the different number of graphene layers. They observed a slightly inferior emission performance from SWCNTs than that from randomly aligned MWCNTs.[32] Their result showed that the degradation of SWCNT emitters was much faster compared with the MWCNT emitters.[18] It is expected that the turn-on field of DWCNTs for electron emission may be as low as that of SWCNTs, and field emission lifetime may be as good as that of MWCNTs because of the unique structure of DWCNTs with small diameters and two graphene layers. The theoretical prediction for field emission of DWCNTs also indicates the strong emission stability due to two neighboring graphene layers.[20] Recently, there have been some reports on the field emission properties of DWCNTs.[33−41] Our group reported field emission properties from DWCNTs dependent on growth temperature.[34] Hiraoka et al. demonstrated that the vertically aligned DWCNTs had an emission current density that was less than 1.0 mA/cm^2.[36] Lee et al. reported field emission performance from screen-printed DWCNT film, showing a turn-on field of 1.33−1.78 V/μm at the emission current density of 1.0 μA/cm^2 and the emission current density of 0.1−1.7 mA/cm^2 at an applied field of about 2.0 V/μm.[38] Ci et al. reported the field emission properties from DWCNT fibers, showing that the low turn-on field of 0.4 V/μm and the high emission current density about 9.0 A/cm^2 at an applied field of about 1.0 V/μm.[39] More recently, our group reported field emission performance dependent on the crystallinity of DWCNTs.[40] In the results, field emission properties were enhanced by increased crystallinity of DWCNTs. However, it is difficult to directly compare the field emission performance of each group's results because the field emission properties largely depend on the CNT emitter structure, the CNT species, the CNT morphology, and field emission measurement techniques. According to overall investigation of field emission properties from DWCNT emitters, they indicated relatively the lower turn-on field and the higher emission current density compared with MWCNTs. Even though there were some reports on field emission of DWCNTs, it is still limited to only simple evaluation of field emission properties. In this work, we tried to investigate a relationship between the field emission properties and the electronic structure of DWCNTs.

The field emission characteristics of SWCNTs and DWCNTs are shown in Figure 6. The typical turn-on field of DWCNTs, which indicates the emission current density of 0.1 μA/cm^2, is about 3.0 V/μm. This turn-on field of DWCNTs is much lower than that of MWCNTs[42,43] but slightly higher than that of SWCNTs.[42,44] The emission current density of DWCNTs reaches about 10 mA/cm^2 at an applied field of about 6.5 V/μm while the emission current density of SWCNTs shows 2.0 mA/cm^2. As mentioned above, direct comparison of field emission performance is very difficult due to different conditions. However, it is understood that the DWCNTs indicated a similar emission performance compared with the previous DWCNTs.[36−38] By the way, as shown in Figure 6a, the current density of DWCNTs shows much lower level than that of SWCNTs in a low electric field region below 4 V/μm, but it reaches a slightly higher level in a medium electric field region of 4−6 V/μm.

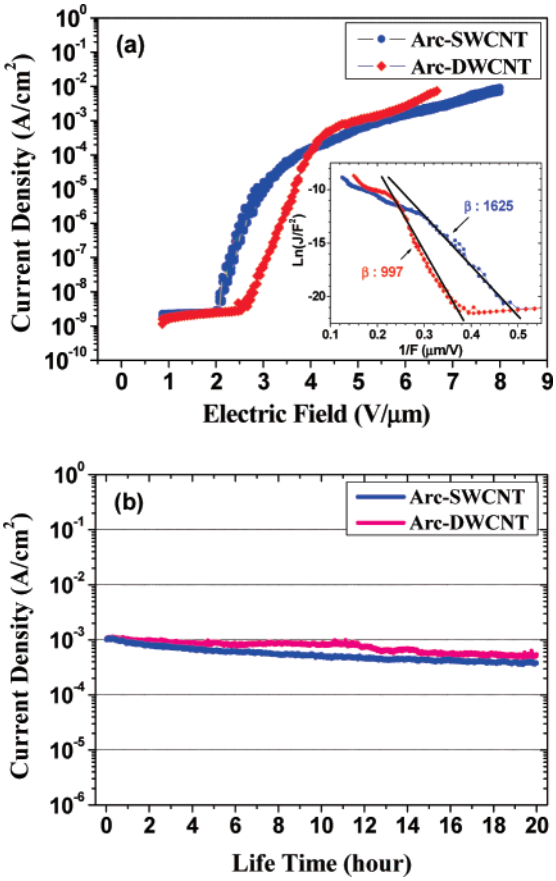

Figure 6. (a) Emission current densities from purified DWCNTs and SWCNTs[23] positioned on Ti/Cr/Si substrate. The inset shows the corresponding Fowler−Nordheim plots. (b) The lifetime measurements of purified DWCNTs and SWCNTs.

However, it achieves a much higher level in a high electric-field region over 6 V/μm.

It is well-known that the field-emission properties of CNTs are influenced by the electronic DOS of valence bands near Fermi level.[21,32] The DWCNTs show lower electronic DOS than that of SWCNTs in the binding energy of 0−3.88 eV, resulting in a higher turn-on field compared with that of SWCNTs. However, the emission current of DWCNTs is higher than that of SWCNTs at high electric field because the occupied level in the binding energy region of 3.88−16.23 eV below Fermi energy can contribute to electron emission at high electric field.[21,32,45−48] This result agrees well with photoemission properties of DWCNTs as shown in Figure 5a. We consider that the higher current density of DWCNTs is mainly attributed to the emitted delocalized graphite σ and σ/π state electron of DWCNTs. The inset shows the corresponding Fowler−Nordheim plots of DWCNTs and SWCNTs, respectively. DWCNTs indicate a lower field enhancement factor than that of SWCNTs. It is well-known that SWCNTs, which generally have smaller diameters than those of DWCNTs, indicate a high aspect ratio, resulting in a higher field enhancement factor.[35]

Figure 6b shows the lifetime measurement of the field emission from DWCNTs, indicating good emission stability for 11 h without degradation but slight degradation in the interval of 11−20 h. According to our result, DWCNTs show a higher emission stability than that of SWCNTs because of two neighboring graphene layers. We suggest that the DWCNTs produced by arc discharge can be used as robust field emitters for various field emission devices.

4. Conclusions

High-purity DWCNTs were synthesized by arc-discharge methods over Fe catalyst and FeS promoter in hydrogen ambient. The synthesized DWCNTs had the outer diameters in the range of 3.0−3.4 nm and the average interlayer distance of 0.38 nm between graphene layers. Our results demonstrated that FeS played a key role for the synthesis of DWCNTs in a hydrogen environment. By adding sulfur into Fe catalyst, it was possible to selectively grow DWCNTs or SWCNTs.

We could find that field emission properties had a close relationship with the electronic structure of DWCNTs. We observed that DWCNTs indicated a higher binding energy of C-1s level than for SWCNTs due to the interlayer, and DWCNTs exhibited a slightly lower intensity than that for SWCNTs in the binding energy region of 0−3.88 eV. The typical turn-on field of DWCNTs, which indicates the emission current density of 0.1 μA/cm^2, is about 3.0 V/μm. The emission current density of DWCNTs reaches about 10 mA/cm^2 at an applied field of about 6.5 V/μm while the emission current density of SWCNTs shows 2.0 mA/cm^2. The higher turn-on field of DWCNTs compared with SWCNTs was caused by lower electronic DOS of valence bands near Fermi level. However, the higher emission current density of DWCNTs was mainly attributed to the emitted delocalized graphite σ and σ/π state electrons of DWCNTs. Moreover, DWCNTs have higher emission stability than that of SWCNTs due to two neighboring graphene layers. We suggest that the DWCNTs produced by arc discharge can have various field emission applications such as field emission displays, flat lamps, X-ray sources, and electron beam sources.

Acknowledgment. This work was supported by the SRC program of Center for Nanotubes and Nanostructured Composites of MOST/KOSEF and supported by the Ministry of Commerce, Industry, and Energy of Korea through a Components and Materials Technology Development project and supported by the Korea Foundation for International Cooperation of Science & Technology (KICOS) through a grant provided by the Korean Ministry of Science &Technology (MOST) in K20601000002-07E0100-00220.

References and Notes

(1) Saito, R.; Dresselhaus, G.; Dresselhaus, M. S. *J. Appl. Phys.* **1993**, *73*, 494.
(2) Lyu, S. C.; Liu, C.; Yang, C. W.; Park, C. Y.; Lee, C. J. *Chem. Mater.* **2003**, *15*, 3951.
(3) Liu, C.; Lyu, S. C.; Lee, T. J.; Choi, S. K.; Eum, S. J.; Yang, C. W.; Park, C. Y.; Lee, C. J. *Chem. Phys. Lett.* **2003**, *373*, 475.
(4) Lyu, S. C.; Lee, T. J.; Yang, C. W.; Lee, C. J. *Chem. Commun.* **2003**, 1404.
(5) Lyu, S. C.; Liu, B. C.; Lee, T. J.; Liu, Z. Y.; Yang, C. W.; Park, C. Y.; Lee, C. J. *Chem. Commun.* **2003**, 734.
(6) Endo, M.; Hayahi, T.; Muramatsu, H.; Kim, Y.-A.; Torrones, H.; Terrones, M.; Dresselhaus, M. S. *Nano Lett.* **2004**, *4*, 1451.
(7) Hertel, T.; Hagen, A.; Talalaev, V.; Arnold, K.; Hennrich, F.; Kappes, M.; Rosenthal, S.; McBride, J.; Ulbricht, H.; Flahaut, E. *Nano Lett.* **2005**, *5*, 511.
(8) Xiong, G. Y.; Suda, Y.; Wang, D. Z.; Huang, J. Y.; Ren, Z. F. *Nanotechnology* **2005**, *16*, 532.
(9) Hutchison, J. L.; Kiselev, N. A.; Krinichnaya, E. P.; Krestinin, A. V.; Loutfy, R. O.; Morawsky, A. P.; Muradyan, V. E.; Obraztsova, E. D.; Sloan, J.; Terekhov, S. V.; Zakharov, D. N. *Carbon* **2001**, *39*, 761.
(10) Saito, Y.; Nakahira, T.; Uemura, S. *J. Phys. Chem. B* **2003**, *107*, 931.
(11) Huang, H.; Kajiura, H.; Tsutsui, S.; Murakami, Y.; Ata, M. *J. Phys. Chem. B* **2003**, *107*, 8794.
(12) Sugai, T.; Yoshida, H.; Shimada, T.; Okazaki, T.; Shinohara, H. *Nano Lett.* **2003**, *3*, 769.
(13) Endo, M.; Muramatsu, H.; Hayashi, T.; Kim, Y. A.; Terrones, M.; Dresselhaust, M. S. *Nature* **2005**, *433*, 476.
(14) Saito, R.; Matsuo, R.; Kimura, T.; Dresselhaus, G.; Dresselhaus, M. S. *Chem. Phys. Lett.* **2001**, *348*, 187.
(15) Hashimoto, A.; Suenaga, K.; Urita, K.; Shimada, T.; Sugai, T.; Bandow, S.; Shinohara, H.; Ijima, S. *Phys. Rev. Lett.* **2005**, *94*, 045504.
(16) Rinzler, A. G.; Hafner, J. H.; Nikolaev, P.; Lou, L.; Kim, S. G.; Tomanek, D.; Colbert, D.; Smalley, R. E. *Science* **1995**, *269*, 1550.
(17) De Heer, W. A.; Chatelain, A.; Ugarte, D. *Science* **1995**, *270*, 1179.
(18) Bonard, J.-M.; Salvetat, J.-P.; Stöckli, T.; De Heer, W. A.; Forró, L.; Châtelain, A. *Appl. Phys. Lett.* **1998**, *73*, 918.
(19) Ren, Z. F.; Huang, Z. P.; Xu, J. W.; Wang, J. H.; Bush, P.; Siegal, M. P.; Provencio, P. N. *Science* **1998**, *282*, 1105.
(20) Son, Y.-W.; Oh, S.; Ihm, J.; Han, S. *Nanotechnology* **2005**, *16*, 125.
(21) Lovall, D.; Buss, M.; Graugnard, E.; Andres, R. P.; Reifenberger, R. *Phys. Rev. B* **2000**, *61*, 5683.
(22) Kociak, M.; Suenage, K.; Hirahara, K.; Saito, Y.; Nakahira, T.; Ijiima, S. *Phys. Rev. Lett.* **2002**, *89*, 155501.
(23) Ha, B.; Park, J.; Kim, S. Y.; Lee, C. J. *J. Phys. Chem. B* **2006**, *110*, 23742.
(24) Kim, P.; Odom, T. W.; Huang, J.-L.; Lieber, C. M. *Phys. Rev. Lett.* **1999**, *82*, 1225.
(25) Saito, Y.; Nakahira, T.; Uemura, S. *J. Phys. Chem. B* **2003**, *107*, 931.
(26) Ren, W.; Li, F.; Chen, J.; Bai, S.; Cheng, H. M. *Chem. Phys. Lett.* **2002**, *359*, 196.
(27) Bandow, S.; Takizawa, M.; Hirahara, K.; Yudadaka, M.; Iijima, S. *Chem. Phys. Lett.* **2001**, *337*, 48.
(28) Kiang, C. H.; Goddard, W. A., III; Beyers, R.; Salem, J. R.; Bethune, D. S. *J. Phys. Chem.* **1994**, *98*, 6612.
(29) Ci, L.; Rao, Z.; Zhou, Z.; Tang, D.; Yan, X.; Liang, Y.; Liu, D.; Yuan, H.; Zhou, W.; Wang, G.; Liu, W.; Xie, S. *Chem. Phys. Lett.* **2002**, *359*, 63.
(30) Zhu, H.; Xu, C.; Wei, B.; Wu, D. *Carbon* **2002**, *40*, 2021.
(31) Wei, J.; Ci, L.; Jiang, B.; Li, Y.; Zhang, X.; Zhu, H.; Xu, C.; Wu, D. *J. Mater. Chem.* **2003**, *13*, 1340.
(32) Bonard, J.-M.; Kind, H.; Stöckli, T.; Nilsson, L.-O. *Solid-State Elec.* **2001**, *45*, 893.
(33) Seko, K.; Kinoshita, J. I.; Saito, Y. *Jpn. J. Appl. Phys.* **2005**, *44*, L743.
(34) Kim, S. Y.; Lee, J. Y.; Park, J.; Park, C. J.; Lee, C. J.; Shin, H. J. *Chem. Phys. Lett.* **2006**, *420*, 271.
(35) Jung, S. I.; Choi, J. S.; Shim, H. C.; Kim, S.; Jo, S. H.; Lee, C. J. *Appl. Phys. Lett.* **2006**, *89*, 233108.
(36) Hiraoka, T.; Yamada, T.; Hata, K.; Futaba, D. N.; Kurachi, H.; Uemura, S.; Yumura, M.; Iijima, S. *J. Am. Chem. Soc.* **2006**, *128*, 13338.
(37) Machida, H.; Honda, S. I.; Ohkura, S.; Oura, K.; Inakura, H.; Katayama, M. *Jpn. J. Appl. Phys.* **2006**, *45*, 1044.
(38) Lee, Y. D.; Lee, H. J.; Han, J. H.; Yoo, J. E.; Lee, Y. H.; Kim, J. K.; Nahm, S.; Ju, B. K. *J. Phys. Chem. B* **2006**, *110*, 5310.
(39) Ci, L.; Punbusayakul, N.; Wei, J.; Vajtai, R.; Talapatra, S.; Ajayan, P. M. *Adv. Mater.* **2007**, *19*, 1719.
(40) Jung, S. I.; Jo, S. H.; Moon, H. S.; Kim, J. M.; Zang, D. S.; Lee, C. J. *J. Phys. Chem. C* **2007**, *111*, 4175.
(41) Somani, P. R.; Somani, S. P.; Lau, S. P.; Flahaut, E.; Tanemura, M.; Umeno, M. *Solid-State Electron.* **2007**, *51*, 788.
(42) Sveningsson, M.; Morjan, R.-E.; Nerushev, O. A.; Sato, Y.; Bäckström, J.; Campbell, E. E. B.; Rohmund, F. *Appl. Phys. A* **2001**, *73*, 409.
(43) Bonard, J.-M.; Salvetat, J.-P.; Stöckli, T.; De Heer, W. A.; Forró, L.; Châtelain, A. *Appl. Phys. A* **1999**, *69*, 245.
(44) Ha, B.; Lee, C. J. *Appl. Phys. Lett.* **2007**, *90*, 23108.
(45) Suzuki, S.; Watanabe, Y.; Kiyokura, T.; Nath, K. G.; Ogino, T.; Heun, S.; Zhu, W.; Bower, C.; Zhou, O. *Phys. Rev. B* **2001**, *63*, 245418.
(46) Suzuki, S.; Bower, C.; Kiyokura, T.; Nath, K. G.; Watanabe, Y.; Zhou, O. *J. Elec. Spec. Relat. Phenom.* **2001**, *114*, 225.
(47) Choi, H. C.; Kim, S. Y.; Jang, W. S.; Bae, S. Y.; Park, J. H.; Kim, K. L.; Kim, K. *Chem. Phys. Lett.* **2004**, *399*, 255.
(48) Schlesser, R.; Collazo, R.; Bower, C.; Zhou, O.; Sitar, Z. *Diamond Relat. Mater.* **2000**, *9*, 1190.